Available online at www.sciencedirect.com
ScienceDirect
Journal of Solid State Chemistry 180 (2007) 2798–2807
JOURNAL OF SOLID STATE CHEMISTRY
www.elsevier.com/locate/jssc

Crystal structures and dielectric properties of ordered double perovskites containing Mg^{2+} and Ta^{5+}

Young-Il Kim*, Patrick M. Woodward

Department of Chemistry, The Ohio State University, Columbus, OH 43210, USA

Received 5 June 2007; received in revised form 9 August 2007; accepted 9 August 2007
Available online 23 August 2007

Abstract

The ordered double perovskites ALaMgTaO$_6$ (A = Ba, Sr, Ca) and La$_2$Mg(Mg$_{1/3}$Ta$_{2/3}$)O$_6$ have been prepared and characterized. Synchrotron X-ray powder diffraction analyses show that all four compounds exhibit a rock-salt type ordering of the B-site cations (Mg^{2+}/Ta^{5+}) and a random distribution of A-site cations (A^{2+}/La^{3+}). The space group symmetries are determined to be $Fm\bar{3}m$ for BaLaMgTaO$_6$, and $P2_1/n$ for SrLaMgTaO$_6$, CaLaMgTaO$_6$, and La$_2$Mg(Mg$_{1/3}$Ta$_{2/3}$)O$_6$. Diffuse-reflectance spectroscopy shows these ordered perovskites have optical band gaps in the range of 4.6–4.8 eV. These values are roughly 1 eV wider than the ternary perovskite oxides of Ta^{5+} such as KTaO$_3$, due to narrowing of the conduction bandwidth which results from Mg^{2+}/Ta^{5+} ordering. These compounds are insulators with dielectric permittivities of $\kappa = 18$–23, dielectric losses of $\tan\delta = 0.004$–0.007, and small temperature coefficients of capacitance <100 ppm/K over the temperature range 20–150 °C. BaLaMgTaO$_6$ is of particular interest because it possesses a near-zero temperature dependence of capacitance.

Keywords: Complex perovskite; Cation ordering; Dielectric

1. Introduction

The physical and chemical characteristics of oxide perovskites AMO_3 are closely tied to the identity and coordination environment of octahedral B-site cation M. Changes in the chemical identity of this cation impact the symmetry, energy and population of the frontier orbitals as well as important structural characteristics, such as deformation/tilting of MO_6 octahedra. The choice of B-site cation is therefore of crucial importance for chemical design of the electrical, magnetic, and mechanical properties. The properties of complex perovskites having multiple cation types at the octahedral site, $AM'_xM''_{1-x}O_3$, are also sensitive to the distribution of M' and M'' cations over the octahedral sites. When the charge and/or size of the M' and M'' cations are sufficiently distinct $AM'_{1/2}M''_{1/2}O_3$ compositions adopt a 1:1 ordering of these cations, with alternating layers of M' and M'' cations along the [111] axis of the cubic perovskite cell [1,2]. This type of ordering yields a structure where the unit cell is doubled and the space group symmetry changes from $Pm\bar{3}m$ to $Fm\bar{3}m$. The three-dimensional arrangement of M' and M'' cations has the same topology as the anions and cations in the rock-salt structure. Consequently, this type of ordering is often called rock-salt type ordering.

$AM'_{1/3}M''_{2/3}O_3$ perovskites can exhibit a 1:2 ordering where the layer repeat sequence along the [111] axis is $\{M'/M''/M''\}$, resulting in hexagonal $P\bar{3}m1$ ($a\approx\sqrt{2}a_p$, $c\approx\sqrt{3}a_p$) space group symmetry. Not all $AM'_{1/3}M''_{2/3}O_3$ perovskites exhibit a 1:2 pattern of ordering. In some cases a non-stoichiometric 1:1 type ordering is preferred, where one of the octahedral sites is fully occupied by the M'' cation and the other site is statistically occupied by the M' cation and the remaining M'' cations [2,3]. Random distributions of the octahedral site cations as well as partially ordered distributions are also observed. Because the cation distributions directly affect the electronic and/or magnetic

*Corresponding author. Present address: Materials Research Laboratory, University of California, Santa Barbara, CA 93106-5121, USA. Fax: +1 805 893 8797.
E-mail address: ykim@mrl.ucsb.edu (Y.-I. Kim).

0022-4596/$ - see front matter © 2007 Elsevier Inc. All rights reserved.
doi:10.1016/j.jssc.2007.08.003

coherences within the extended lattice, it is important to understand and control cation ordering in complex perovskites [4].

For many decades perovskites containing d^0 cations, such as Ta^{5+}, Nb^{5+}, and Ti^{4+}, have been utilized for their attractive dielectric properties. With the exception of those perovskites containing a lone pair cation on the A-site (i.e. Pb^{2+}) the $AM'_xM''_{1-x}O_3$ (M'' = Ta, Nb) perovskites usually adopt centrosymmetric structures. Consequently, they are not ferroelectrics. Nevertheless, they may possess relatively large dielectric permittivities (~20–50) originating from electronic polarization mechanisms. Complex perovskites based on tantalum tend to exhibit smaller dielectric constants (κ), smaller loss factors ($\tan\delta$), and smaller temperature coefficients of dielectric constant (τ_κ) and resonant frequency (τ_f) than the corresponding niobium analogs. In particular, $BaM'_{1/3}Ta_{2/3}O_3$ (M' = Mg, Zn) compounds exhibit low losses (high quality factors) and low temperature coefficients. This makes them preferred compounds for fabricating dielectric resonators and band-pass filters in microwave integrated circuits [5,6]. Studies of niobium compounds have tended to focus on the development of new $PbM'_xNb_{1-x}O_3$ relaxor materials [7]. It should be noted that the dielectric behaviors of complex perovskites can vary significantly depending upon the extent of both cation ordering and octahedral tilting. Empirically, the lower dielectric loss has been associated with the higher degree of cation ordering, while the more negative τ_f has been associated with the lack of octahedral tilting [8,9].

In this work, we explore the structural and dielectric properties of Mg/Ta complex perovskites, ALaMgTaO$_6$, (A = Ba, Sr, Ca) and $La_2Mg(Mg_{1/3}Ta_{2/3})O_6$. Their crystal symmetries, optical band gaps and the dielectric behaviors are compared with compositionally related perovskites, such as $Ba_3MgTa_2O_9$, $Ba_3ZnTa_2O_9$ and Ba_2ScTaO_6.

2. Experimental

All compounds prepared in this study were synthesized using high purity powder reagents ($BaCO_3$, $SrCO_3$, $CaCO_3$, La_2O_3, MgO, Ta_2O_5, ZnO, Sc_2O_3) as purchased. Lanthanum and magnesium oxides were baked at 900 °C for 10 h before use. Quantitatively weighed reagents were mixed under acetone using agate mortar and pestle, pressed into pellets, and heated in a chamber furnace. In addition to the compounds which are the focus of this study, $Ba_3MgTa_2O_9$, $Ba_3ZnTa_2O_9$ and Ba_2ScTaO_6 were also prepared and characterized. The heat treatments were carried out at 1300–1550 °C for 12–24 h with intermittent grindings. Table 1 lists the final annealing temperature for each composition.

X-ray powder diffraction (XRPD) patterns were collected on the resulting white powder samples using synchrotron X-rays on beamline X7A of the National Synchrotron Light Source (NSLS), located at Brookhaven National Laboratory (BNL). Monochromatic radiation (λ~0.7 Å) was obtained using a Ge 1 1 1 channel cut crystal monochromator. The wavelength was calibrated by a CeO_2 standard. Each sample, packed in a 0.2 or 0.3 mm diameter glass capillary, was spun during data collection for better powder averaging in the Debye–Scherer mode measurement. A gas-proportional linear position sensitive detector was stepped in 0.25° intervals between 3° and 65° to produce 0.01° step scan data. The crystal structures were refined by Rietveld method using the GSAS-EXPGUI software suite [10,11].

Table 1
Syntheses temperatures, long range order parameters, and band gap energies of the complex perovskites containing Ta^{5+}

Formula	T (°C)	S	E_g (eV)
$BaLaMgTaO_6$	1450	>0.99	4.67
$SrLaMgTaO_6$	1400	>0.99	4.75
$CaLaMgTaO_6$	1400	>0.99	4.82
$La_2Mg(Mg_{1/3}Ta_{2/3})O_6$	1475	>0.99	4.55
$Ba_3MgTa_2O_9$	1500	0.91	4.28
$Ba_3ZnTa_2O_9$	1450	0.44	4.32
Ba_2ScTaO_6	1550	0.42	4.19

Diffuse-reflectance absorption spectroscopy was performed using a scanning double-beam spectrometer (Perkin-Elmer Lambda 20) equipped with a 50 mm integrating sphere (Labsphere). The absorption spectra were recorded in the ultraviolet (UV) to visible light range (λ = 200–700 nm) with a commercial $BaSO_4$ disk (Labsphere) as the reference. The band gap energies were determined from Shapiro's method [12] of extrapolating the onset of absorption to the wavelength axis.

The dielectric behavior and electrical conductivity were measured using an impedance analyzer (Solartron SI1260) at 100 kHz, over the temperature range 20–150 °C. For the electrical measurements, each sample was pressed into a 13 mm diameter pellet, which was then sintered at a temperature that was 25 °C above the final annealing temperature. The sintered oxide pellets were 80–82% of their theoretical density. To make electrode contacts, In–Ga eutectic alloy (Alfa, 99.99%, In:Ga 24.5:75.5 wt%) was rubbed on both faces of the pellets which were then placed between Pt plates connected to BNC cables. The measurements were carried out in air using an oil bath for temperature control. Basic solid state impedance theory [13] was used to interpret the measured data and evaluate the dielectric constant, dielectric loss, and the electrical conductivity.

3. Results and discussion

3.1. Synchrotron X-ray powder diffraction

Before discussing the synchrotron XRPD patterns it is helpful to briefly review the impacts of octahedral tilting and cation ordering on the crystal structures of complex perovskites. Most complex perovskites take one of four

common types of crystal symmetry depending on whether they possess octahedral tilting distortion and/or cation ordering [1,14,15]. Compounds with a disordered or random M'/M'' arrangement that do not undergo an octahedral tilting distortion adopt the simple cubic perovskite structure, with $Pm\bar{3}m$ symmetry and an unit edge, $a_p \approx 4$ Å. The most common type of octahedral tilting distortion, $a^-b^+a^-$, lowers the symmetry to orthorhombic *Pnma* with the unit dimensions of $\sqrt{2}a_p \times 2a_p \times \sqrt{2}a_p$ [16]. If 1:1 ordering of M'/M'' cations in the rock-salt arrangement is introduced the crystallographic symmetries change to cubic $Fm\bar{3}m$ symmetry with $a = 2a_p$ (no tilting), or monoclinic $P2_1/n$ symmetry with $a \approx \sqrt{2}a_p$, $b \approx \sqrt{2}a_p$, $c \approx 2a_p$ and $\beta \approx 90^\circ$ ($a^-a^-c^+$ tilting) [16,17].

While the octahedral tilt systems and resulting symmetries discussed in the preceding paragraph are the most common other combinations are sometimes observed. Among the less frequently observed symmetries of rock salt ordered perovskites are the $I4/m$, $I2/m$ and $R\bar{3}$ types, which result from $a^0a^0c^-$, $a^0b^-b^-$, and $a^-a^-a^-$ tilting, respectively [16,17]. Because rock salt ordering of the cations and out-of-phase octahedral tilting give rise to the same set of superstructure reflections it is often difficult to distinguish among these symmetries, particularly from X-ray diffraction data [17,18].

Other types of cation ordering are also possible. A 1:1 ordering where M' and M'' alternate in layers has been observed in Ln_2CuMO_6 ($P2_1/m$, $2a_p \times 2a_p \times 2a_p$) with Ln = La, Pr, Nd, Sm and M = Sn, Zr [19,20]. In the case of 1:2 ordering in $AM'_{1/3}M''_{2/3}O_3$ perovskites the symmetry becomes hexagonal $P\bar{3}m1$ ($a \approx \sqrt{2}a_p$, $c \approx \sqrt{3}a_p$). A discussion of how to identify cation ordering and octahedral tilting in complex perovskites can be found in a number of places in the literature [1,14,17,18].

The first step in analyzing the XRPD patterns is to look for characteristic superstructure reflections and/or peak splitting that can be used to identify the cation ordering and octahedral tilting. The lower 2θ region of the XRPD patterns is shown in Fig. 1. Given the large difference in atomic number between Ta^{5+} and the lower valent cations (Mg^{2+}, Sc^{3+}, Zn^{2+}) a strong pseudocubic 1 1 1 reflection at $d \approx \sqrt{\frac{4}{3}}a_p$ ($2\theta \approx 19^\circ$) is expected if the cations order in a rock salt fashion. This is observed for ALaMgTaO$_6$ (A = Ba, Sr, Ca) and Ba_2ScTaO_6 samples. Among the samples with an $AM'_{1/3}M''_{2/3}O_3$ stoichiometry $Ba_3MgTa_2O_9$ and $Ba_3ZnTa_2O_9$ samples adopt 1:2 cation ordering as expected while $La_3Mg_2TaO_9$ adopts a non-stoichiometric 1:1 cation ordering better written as $La_2Mg(Mg_{1/3}Ta_{2/3})O_6$. As shown in Fig. 2a, the diffraction peaks from BaLaMgTaO$_6$ retain highly symmetric profiles even at the high angle limit, which supports a choice of $Fm\bar{3}m$ symmetry. To trace a possible deviation from the cubic symmetry, the BaLaMgTaO$_6$ structure was examined against an $I4/m$ type model but there were little improvement in the fit ($R_{wp} = 6.42\%$ as compared with 6.57% for $Fm\bar{3}m$) and only a weak tetragonal

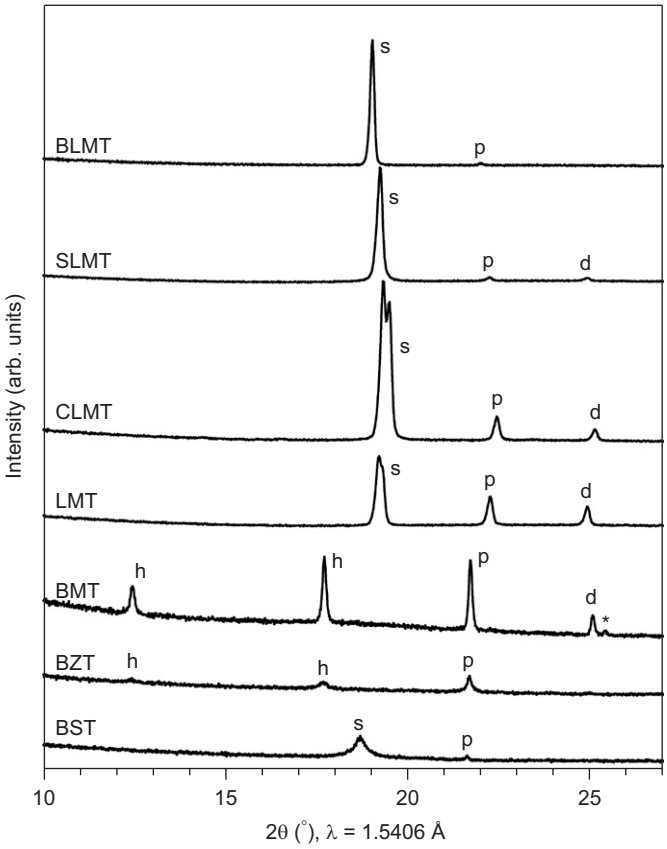

Fig. 1. XRPD patterns at lower 2θ range for the Mg/Ta complex perovskite oxides, BLMT (BaLaMgTaO$_6$), SLMT (SrLaMgTaO$_6$), CLMT (CaLaMgTaO$_6$), LMT ($La_2Mg(Mg_{1/3}Ta_{2/3})O_6$), BMT ($Ba_3MgTa_2O_9$), BZT ($Ba_3ZnTa_2O_9$), and BST ($Ba_2ScTaO_6$). 2θ scales were adjusted to the Cu$K\alpha_1$ wavelength. Peaks are labeled according to the origin of diffraction plane: s—rock-salt type cation ordering, h—1:2 cation ordering, p—primitive cubic edge, d—octahedral tilting, and *—impurity phase.

distortion, $c/(2^{1/2}a) = 1.0012$. While this does not completely rule out $I4/m$ symmetry there is no compelling reason to lower the symmetry. Neutron diffraction data would be needed to definitively assign the symmetry.

On the other hand, the combination of a strong peak at $2\theta \approx 19^\circ$ (psuedocubic 1 1 1 reflection) along with the peak at $2\theta \approx 25^\circ$ (psuedocubic 2 1 0 reflection) are characteristic of $P2_1/n$ symmetry for SrLaMgTaO$_6$, CaLaMgTaO$_6$, and $La_2Mg(Mg_{1/3}Ta_{2/3})O_6$. For these three compounds, other space groups such as $I4/m$ ($a^0a^0c^-$ tilting), $I2/m$ ($a^0b^-b^-$ tilting), and $C2/c$ ($a^0b^+c^-$ tilting) have been also examined. In Fig. 2b the SrLaMgTaO$_6$ XRPD pattern is compared with the allowed peak positions for $C2/c$, $P2_1/n$, $I2/m$, $I4/m$ space group symmetries. The $I4/m$ and $I2/m$ symmetries, for both of which $a \approx \sqrt{2}a_p$, $b \approx \sqrt{2}a_p$, $c \approx 2a_p$, have stricter reflection conditions than $P2_1/n$ symmetry. Accordingly they could be quickly excluded by identifying specific reflections (pseudocubic 2 1 0, 2 1 1, 2 2 1, 3 3 1, etc.), from the experimental XRPD pattern. Apparently $I2/m$ or any other higher symmetry space groups (cubic, tetragonal, orthorhombic, trigonal) cannot account for the observed diffraction pattern of SrLaMgTaO$_6$. The monoclinic $C2/c$

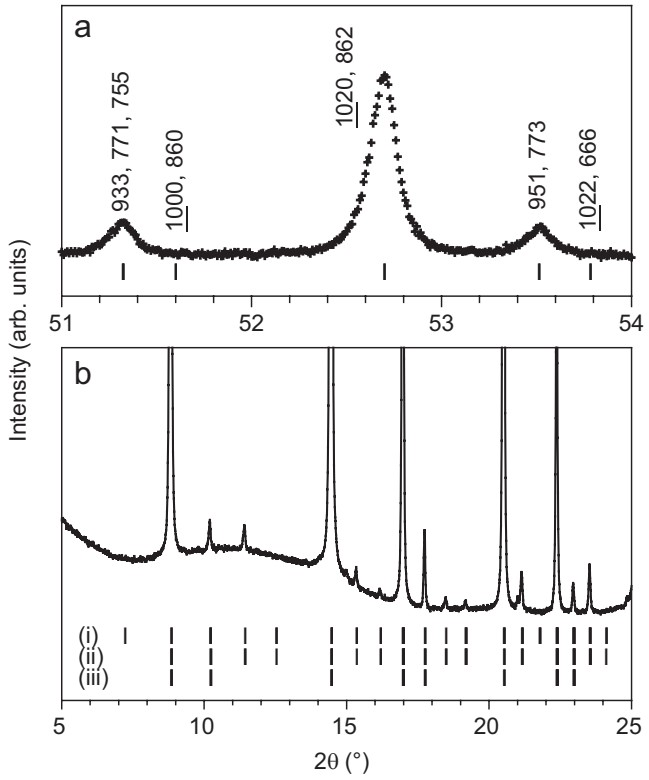

Fig. 2. XRPD patterns of (a) $BaLaMgTaO_6$ at higher angle region and (b) $SrLaMgTaO_6$ as compared with the Bragg reflection positions expected for different space groups, (i) $C2/c$, (ii) $P2_1/n$, and (iii) $I2/m$ and $I4/m$ (these two have the same reflection conditions).

type cell ($a \approx 2a_p$, $b \approx 2a_p$, $c \approx 2a_p$) can generate extra reflections in addition to those associated with $P2_1/n$ symmetry. But none of the pseudocubic 1 1 0 ($2\theta \approx 7.2°$) and 3 3 0/1 1 4 ($2\theta \approx 21.8°$) reflections, which are allowed for $C2/c$ symmetry but not for $P2_1/n$, occur in the experimental pattern. This observation, in conjunction with the scarcity of known double perovskite oxide examples, implies the inadequacy of $C2/c$ symmetry for $SrLaMgTaO_6$. Therefore the Rietveld refinements were performed using the space group symmetries of $Fm\bar{3}m$ for $BaLaMgTaO_6$, and $P2_1/n$ for $SrLaMgTaO_6$, $CaLaMgTaO_6$ and $La_2Mg(Mg_{1/3}Ta_{2/3})O_6$.

Previous studies on $BaLaMgTaO_6$ [21] and $CaLaMgTaO_6$ [22] also described their crystal systems as ordered cubic and monoclinic, respectively, although the atomic positions were not determined. On the other hand, the structures of $SrLaMgTaO_6$ [23] and $La_2Mg(Mg_{1/3}Ta_{2/3})O_6$ [24] have been previously analyzed by Rietveld refinements and reported in the literature. The previous studies assigned the $Fm\bar{3}m$ symmetry to $SrLaMgTaO_6$ and $Pnma$ symmetry to $La_2Mg(Mg_{1/3}Ta_{2/3})O_6$, both in disagreement with our findings. Such discrepancies cannot be clearly traced at present but the superstructure reflections, peak splitting and Rietveld refinement leave little doubt that our samples have the structures assigned in Table 2. For $Ba_3MgTa_2O_9$ and $Ba_3ZnTa_2O_9$ refinements confirmed the reported solutions, $P\bar{3}m1$ [25–27]. The M'/Ta ordering parameter (S) was calculated as follows [28]:

$$S = \frac{(R_i - F_i)}{(1 - F_i)}, \tag{1}$$

where F is the fractional composition of Ta (or M'), and R is its refined occupancy on the presumed crystallographic site. For an example of $La_2Mg_{4/3}Ta_{2/3}O_6$, in which $F_{Mg} = 2/3$ and $F_{Ta} = 1/3$, if its two octahedral sites are occupied as ($Mg_{5/6}Ta_{1/6}$) and ($Mg_{1/2}Ta_{1/2}$), the former is designated as Mg-site, and the latter, Ta-site. Then, $R_{Mg} = 5/6$ and $R_{Ta} = 1/2$, and the S parameter for octahedral Mg/Ta equals 50%.

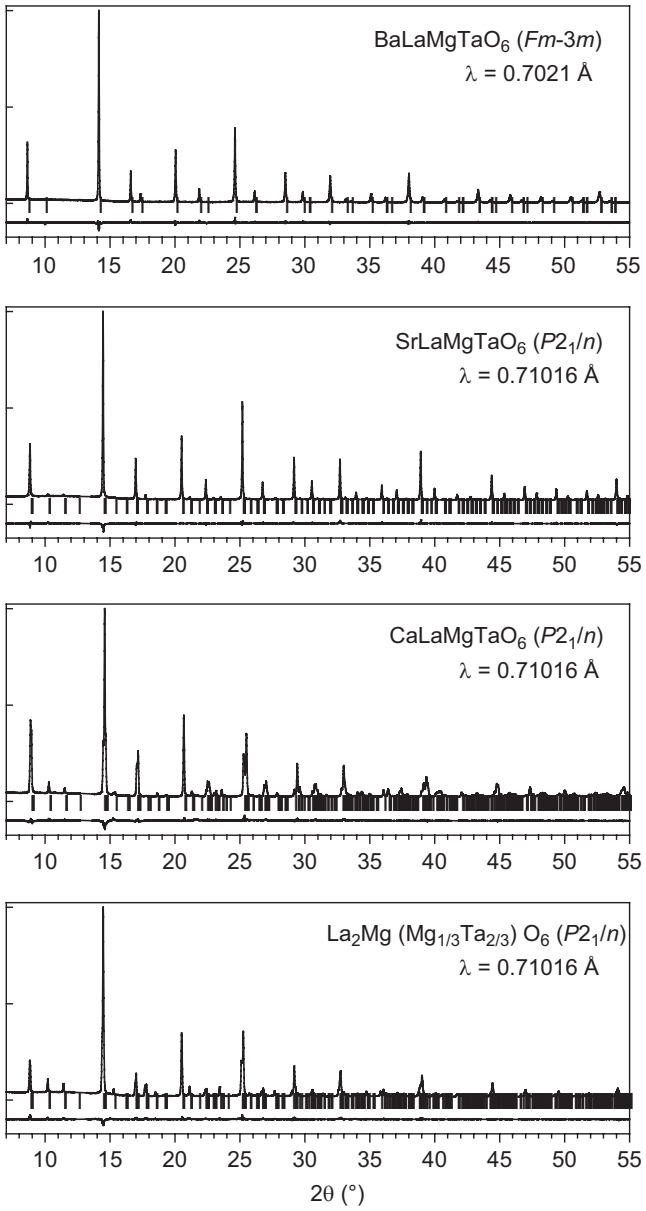

Fig. 3. Rietveld refinements of complex perovskite oxides, $ALaMgTaO_6$ (A = Ba, Sr, Ca), and $La_2Mg(Mg_{1/3}Ta_{2/3})O_6$. Experimental profiles are shown together with the difference patterns and Bragg peak positions at the bottom.

Table 2
Rietveld refinement details for ALaMgTaO$_6$ (A = Ba, Sr, Ca), and La$_2$Mg(Mg$_{1/3}$Ta$_{2/3}$)O$_6$

	ALaMgTaO$_6$			La$_2$Mg(Mg$_{1/3}$Ta$_{2/3}$)O$_6$
	A = Ba	A = Sr	A = Ca	
Radiation (Å)	0.7021	0.710164	0.710164	0.710164
2θ range (deg)	4–55	3–65	5–56	3–56
R_{wp}/ R_p (%)	6.57/5.18	2.98/1.95	3.66/2.96	3.67/2.50
χ^2	2.91	7.65	4.56	3.93
No. reflections	55	948	621	629
No. variables	13	27	27	25
SG	$Fm\bar{3}m$	$P2_1/n$	$P2_1/n$	$P2_1/n$
Z	4	2	2	2
V (Å^3)	524.84(1)	253.730(3)	247.648(7)	253.496(6)
a (Å)	8.06632(6)	5.6407(1)	5.55914(6)	5.61572(5)
b (Å)		5.6425(1)	5.63554(7)	5.66930(1)
c (Å)		7.9720(1)	7.90483(9)	7.96227(7)
β (deg)		89.995(5)	89.948(2)	89.988(3)

The results of the structure refinements (Fig. 3 and Tables 2, 3) show that within experimental error the Ta and Mg atoms are completely ordered in ALaMgTaO$_6$ (A = Ba, Sr, Ca) and La$_2$Mg(Mg$_{1/3}$Ta$_{2/3}$)O$_6$. Ba$_3$MgTa$_2$O$_9$ is also highly ordered, although there appears to be a small amount of site disorder. The degree of ordering is significantly reduced in Ba$_3$ZnTa$_2$O$_9$ and Ba$_2$ScTaO$_6$ (Table 1). Apparently the differences in charge (+5 vs. +2) and size are sufficient to stabilize a highly ordered distribution when M' = Mg^{2+} (r = 0.72 Å) and M'' = Ta^{5+} (r = 0.64 Å) [29]. Interestingly the composition LaMg$_{2/3}$Ta$_{1/3}$O$_3$ favors a non-stoichiometric 1:1 cation ordering, La$_2$Mg(Mg$_{1/3}$Ta$_{2/3}$)O$_6$, over the 1:2 ordering seen for Ba$_3$MgTa$_2$O$_9$ and Ba$_3$ZnTa$_2$O$_9$ despite a stoichiometry which would appear to favor 1:2 ordering. There is a decrease in the degree of cation order upon replacing Mg^{2+} with Zn^{2+} (r = 0.74 Å), to form Ba$_3$ZnTa$_2$O$_9$, which cannot be explained by either formal charge or size comparisons. Both the Ba$_3$MgTa$_2$O$_9$ and Ba$_3$ZnTa$_2$O$_9$ display wide ranges of cation order, which increases with higher sintering temperature and/or longer sintering time [26,30]. This is a clear indication that the degree of disorder is determined by kinetic limitations rather than thermodynamic equilibrium. Since the two phases have different melting points, it is not straightforward to directly compare the ordering tendencies of Ba–Mg–Ta and Ba–Zn–Ta systems. The Sc^{3+} ion (r = 0.745 Å), compared with Mg^{2+} or Zn^{2+}, has a similar size mismatch with Ta^{5+} but a reduced charge difference. The net effect is a reduction in the overall B-site ordering in Ba$_2$ScTaO$_6$. In a previous study the Sc^{3+}/Ta^{5+} ordering in Ba$_2$ScTaO$_6$ was observed as S = 0.51 [18].

The cubic (BaLaMgTaO$_6$, Ba$_2$ScTaO$_6$) and hexagonal (Ba$_3$MgTa$_2$O$_9$ and Ba$_3$ZnTa$_2$O$_9$) compounds where the A-site cation is barium do not exhibit octahedral tilting distortions under ambient conditions. However, the compounds where Ba^{2+} has been replaced by a smaller cation, ALaMgTaO$_6$ (A = Sr, Ca) and La$_2$Mg(Mg$_{1/3}$Ta$_{2/3}$)O$_6$, undergo $a^-a^-c^+$ type octahedral tilting distortions [16]. The octahedral tilting is illustrated for SrLaMgTaO$_6$ in Fig. 4. The presence/absence of octahedral tilting can largely be explained by considering the ion size ratios needed for ideal crystal packing. The tolerance factor (t) of complex perovskite oxides can be defined as

$$t = \frac{(\langle r_A \rangle + r_O)}{\sqrt{2}(\langle r_M \rangle + r_O)}, \quad (2)$$

where $\langle r \rangle$ is the composition-weighted ion radius at the given site. Because the calculated t values for Ba$_2$ScTaO$_6$ (1.017), Ba$_3$MgTa$_2$O$_9$ (1.030) and Ba$_3$ZnTa$_2$O$_9$ (1.027) are larger than unity octahedral tilting is not expected for these compositions. On the other hand, based on the tolerance factor alone (0.981), one might expect an octahedral tilting distortion for BaLaMgTaO$_6$. However, the lack of tilting in a double perovskite with t<1 is not unprecedented. It was recently confirmed by neutron diffraction that Ba$_2$YNbO$_6$ (t = 0.981) is also cubic at room temperature [18]. As t gets smaller $a^-a^-c^+$ tilting becomes energetically favored and monoclinic symmetry is observed in SrLaMgTaO$_6$ (t = 0.952), CaLaMgTaO$_6$ (t = 0.935), and La$_2$Mg(Mg$_{1/3}$Ta$_{2/3}$)O$_6$ (t = 0.932). The degree of distortion in each compound, estimated from the bond angles of (Ta−O−M') and the octahedral tilting angles, correlates reasonably well with the deviation of t from 1. The evolution of the unit cell volumes can also be understood from the component ions' sizes. The three ALaMgTaO$_6$ type compounds did not exhibit any indication of A/La ordering. This is not unexpected as ordering of A-site cations is rare. Nonetheless, it has been observed in a few cases [31–34].

In Table 4, the Mg–O and Ta–O distances are compared for the compounds studied in this work and a recently reported A-site deficient perovskite La$_{5/3}$MgTaO$_6$ [35]. In general there are good agreements with the expected distances of 1.99 Å (Ta–O) and 2.07 Å (Mg–O) based on 6-coordinate cation and 2-coordinate anion ionic radii [29]. In terms of distance the only outlier is BaLaTaMgO$_6$ where the Ta–O distance is somewhat smaller than expected. The apparent contraction of the Ta–O bonds may be a response to the bond stresses that result when the tolerance factor

Table 3
Atomic parameters for ALaMgTaO$_6$ (A = Ba, Sr, Ca), and La$_2$Mg(Mg$_{1/3}$Ta$_{2/3}$)O$_6$, together with interatomic distances and angles for selected bonds[a]

		ALaMgTaO$_6$			La$_2$Mg(Mg$_{1/3}$Ta$_{2/3}$)O$_6$
		A = Ba	A = Sr	A = Ca	
A/La	x	$\frac{1}{4}$	0.506(1)	0.5092(5)	0.5100(3)
	y	$\frac{1}{4}$	0.5215(1)	0.5368(1)	0.5363(1)
	z	$\frac{1}{4}$	0.2456(7)	0.2504(1)	0.2506(1)
	U_{iso} (Å^2)	0.0098(5)	0.0027(4)	0.0032(2)	0.004(1)
	Occu.	Ba$_{0.5}$La$_{0.5}$	Sr$_{0.5}$La$_{0.5}$	Ca$_{0.5}$La$_{0.5}$	La$_{1.0}$
M1	x, y, z	$\frac{1}{2}$, $\frac{1}{2}$, $\frac{1}{2}$	$\frac{1}{2}$, 0, 0	$\frac{1}{2}$, 0, 0	$\frac{1}{2}$, 0, 0
	U_{iso} (Å^2)	0.0068(3)	0.0052(1)	0.0003(1)	0.003(1)
	Occu.	Ta$_{1.000(3)}$	Ta$_{1.000(2)}$	Ta$_{1.000(2)}$	Ta$_{0.67(1)}$Mg$_{0.33(1)}$
M2	x, y, z	0, 0, 0	0, $\frac{1}{2}$, 03	0, $\frac{1}{2}$, 03	0, $\frac{1}{2}$, 03
	U_{iso} (Å^2)	0.012(1)	0.014(1)	0.0016(9)	0.003(1)
	Occu.	Mg$_{1.000(3)}$	Mg$_{1.000(2)}$	Mg$_{1.000(2)}$	Mg$_{1.00(1)}$
O1	x	0.2593(5)	0.244(3)	0.207(1)	0.214(2)
	y	0	0.240(3)	0.195(1)	0.203(2)
	z	0	−0.037(2)	−0.047(1)	−0.041(2)
	U_{iso} (Å^2)	0.023(2)	0.0107(7)	0.007(1)	0.002(1)
O2	x		0.288(3)	0.299(2)	0.290(2)
	y		0.721(3)	0.715(1)	0.717(2)
	z		−0.032(3)	−0.048(1)	−0.044(2)
	U_{iso} (Å^2)		0.0107(7)	0.007(1)	0.002(1)
O3	x		0.422(3)	0.423(1)	0.423(1)
	y		−0.011(2)	−0.017(1)	−0.0136(9)
	z		0.249(2)	0.248(1)	0.249(1)
	U_{iso} (Å^2)		0.0107(7)	0.007(1)	0.002(1)
d_{M1-O} (Å)		(6 ×) 1.941(4)	(2 ×) 2.00(1)	(2 ×) 1.999(9)	(2 ×) 2.002(9)
			(2 ×) 1.99(1)	(2 ×) 1.993(8)	(2 ×) 2.024(9)
			(2 ×) 2.03(1)	(2 ×) 2.008(8)	(2 ×) 2.032(10)
d_{M2-O} (Å)		(6 ×) 2.092(4)	(2 ×) 2.03(1)	(2 ×) 2.102(8)	(2 ×) 2.096(9)
			(2 ×) 2.06(1)	(2 ×) 2.090(8)	(2 ×) 2.070(9)
			(2 ×) 2.05(1)	(2 ×) 2.041(8)	(2 ×) 2.045(10)
$\angle_{M1-O-M2}$ (deg)		(3 ×) 180	(1 ×) 162.9(9)	(1 ×) 149.6(5)	(1 ×) 153.6(7)
			(1 ×) 159(1)	(1 ×) 151.6(5)	(1 ×) 154.1(7)
			(1 ×) 154.9(8)	(1 ×) 154.9(4)	(1 ×) 155.2(4)
θ (deg)[b]	M1	0	10.6	14.5	13.4
	M2	0	10.4	14.0	13.1
ϕ (deg)[b]	M1	0	10.3	12.5	11.6
	M2	0	10.1	12.0	11.3

[a] A-site occupancies were not refined, whereas the B-site occupancy sums were constrained to 1.
[b] Octahedral tilt angles θ and ϕ, respectively, denoting the rotations about (110) and (001) axes of aristotype perovskite, were calculated from the lattice constants and M–O bond distances using a software TUBERS [15].

dips below 1. However, the observation that the Mg–O distance is somewhat longer than seen for the other perovskites raises the possibility that the refined oxygen position may be slightly off. Neutron diffraction would be needed to confirm the contraction of the Ta–O bonds in this compound.

The small values of the octahedral distortion index, Δ_d [36], show that the octahedra remain quite symmetric despite the reduction in symmetry. This is not unusual for ordered perovskites. Easily the most distorted octahedron is the Ta site in Ba$_3$MgTa$_2$O$_9$. In $A_3M'M''_2O_9$ perovskites there are two chemically distinct oxygen sites. Two-thirds of the oxygen atoms sit in between the M' and M'' layers, whereas the remaining one-third sits in between two M'' layers. In Ba$_3$MgTa$_2$O$_9$ two-thirds of the oxygens make one bond to Mg^{2+} and another to Ta^{5+}, while the remaining oxygens make two bonds to Ta^{5+}. This leads to a bonding instability because the oxygen that makes two bonds with Ta^{5+} is overbonded. The instability can be alleviated if the Ta^{5+} ions shift away from the overbonded

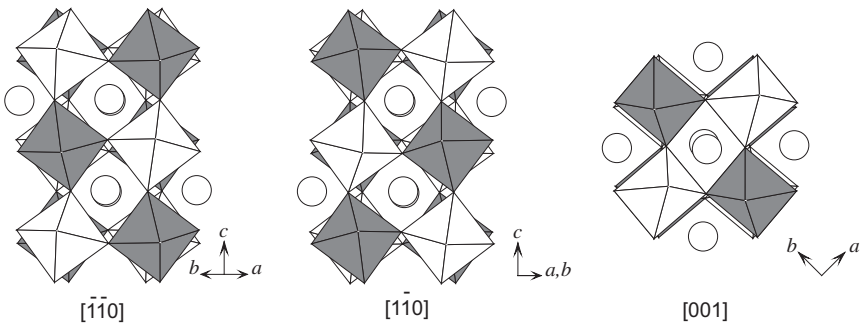

Fig. 4. Octahedral tilts in $SrLaMgTaO_6$ viewed along the three orthonormal axes (tilt system symbol: $a^-a^-c^+$). Sr/La are represented by circles, and the MgO_6 and TaO_6 octahedra are shown in white and gray, respectively. $CaLaMgTaO_6$ and $La_2Mg(Mg_{1/3}Ta_{2/3})O_6$ are isostructural with $SrLaMgTaO_6$.

Table 4
Intraoctahedral distortions[a] in Mg/Ta complex perovskites.

	Mg–O		Ta–O	
	$\langle d\rangle$ (Å)	$10^4\Delta_d$	$\langle d\rangle$ (Å)	$10^4\Delta_d$
$BaLaMgTaO_6$	2.092	0	1.941	0
$SrLaMgTaO_6$	2.047	0.37	2.007	0.72
$CaLaMgTaO_6$	2.078	1.61	2.000	0.09
$La_{5/3}MgTaO_6$ [35]	2.062	0.28	1.968	1.67
$La_2Mg(Mg_{1/3}Ta_{2/3})O_6$	2.070	1.01	2.019	0.39
$Ba_3MgTa_2O_9$	2.076	0	2.028	9.05

[a]Distortion index is defined as $\Delta_d = (1/6)\sum_{i=1-6}[(d_i - \langle d\rangle)/\langle d\rangle]^2$, where d_i is the length of each $M-O$ bond, and $\langle d\rangle$, the average of six d_i's.

oxygen toward the opposite face of the octahedron. Such distortions are energetically favored for d^0 cations such as Ta^{5+} and Nb^{5+}, as well as for lone pair ions like Bi^{3+} [37]. Thus 1:2 ordering is generally favorable for $Ba_3M'Ta_2O_9$ compositions. However, in $La_3Mg_2TaO_9$ the bonding instability that would result from 2:1 ordering occurs at the underbonded oxygen ions shared by two Mg^{2+} ions. The electronic configuration of a Mg^{2+} ($[Ne]3s^0$) is not conducive to a displacement toward the underbonded oxygen. Hence non-stoichiometric 1:1 ordering ($La_2Mg(Mg_{1/3}Ta_{2/3})O_6$) is favored over 2:1 ordering ($La_3Mg_2TaO_9$).

3.2. Optical band gaps

The optical band gaps (E_g) were determined by diffuse-reflectance absorption spectroscopy in the wavelength range of 200−700 nm as shown in Fig. 5, and listed in Table 1. The complex perovskites studied here possess band gaps that are larger than those of related ternary perovskite tantalates, such as $KTaO_3$ ($E_g = 3.5$ eV) [38]. As indicated by the XRPD analyses, all of the 1:1 ordered Mg/Ta complex oxide samples have essentially complete cation ordering, so that each TaO_6 octahedra is neighbored by MgO_6 at all the six corners. In such a configuration the spatial overlaps and electronic interactions of Ta 5*d* and O 2*p* orbitals are localized due to the fact that the Mg 3*s* orbital has neither the correct symmetry or energy to mix

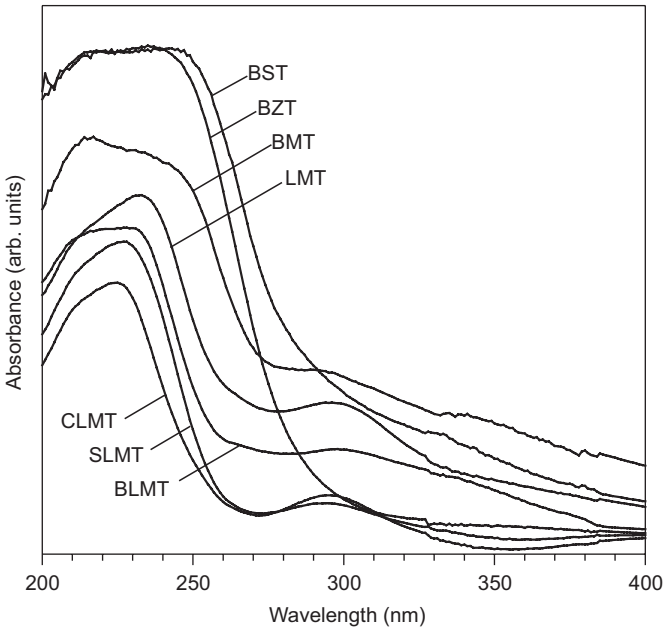

Fig. 5. UV–visible absorption spectra for Mg/Ta complex perovskite oxides. Compositions are abbreviated to same acronyms as in Fig. 1.

with the Ta 5*d*–2*p* π^* interactions that characterize the lower energy region of the conduction band [38]. The virtual electronic isolation of TaO_6 octahedra leads to a narrowing of the conduction bandwidth and a corresponding increase in band gap with respect to the continuous Ta−O−Ta network that exists in $ATaO_3$ perovskites. Because the bandwidths are already narrowed by cation ordering and the local TaO_6 octahedra are rather similar from one compound to the next the band gap energies of the ordered perovskites are not very sensitive to octahedral tilting distortions.

The band gaps of the reference compounds $Ba_3MgTa_2O_9$, $Ba_3ZnTa_2O_9$, Ba_2ScTaO_6 are intermediate between the 1:1 ordered perovskites and the ternary perovskites ($KTaO_3$, $NaTaO_3$). The 1:2 ordering found for $Ba_3MgTa_2O_9$ and $Ba_3ZnTa_2O_9$ retains the Ta–O–Ta connectivity in two dimensions. This should lead to a reasonable conduction bandwidth in some reciprocal space directions.

However, even in those directions the Ta^{5+} displacements lower the symmetry and reduce the bandwidth with respect to the cubic $KTaO_3$ structure. Ba_2ScTaO_6 displays the least long range order of M'/Ta (Table 1), raising the possibility for Ta–O–Ta pathways and linkages. This would lower the band gap somewhat, in which the exact amount depends upon the nature of the disorder on a short to intermediate range scale. Additionally it should be noted that the energy and symmetry of the $3d$ valence orbitals on Sc^{3+} are comparable in energy (−9.35 eV) to those of the $5d$ valence orbitals on Ta^{5+} (−9.57 eV) [39]. This should facilitate Sc $3d$–O$2p$–Ta $5d$ orbital mixing. A previous density functional electronic structure calculation has suggested that the Sc and Ta will make nearly equivalent contributions to the conduction band of fully ordered Ba_2ScTaO_6, thereby leading to a larger conduction band width (vs. Mg/Ta ordered perovskites) [38]. In several of the spectra shown in Fig. 5, pre-edge absorption peaks are found at 295–300 nm (ca. 4.15 eV). Similar sub-band gap excitations have been observed in other wide band gap double perovskites [38].

3.3. Dielectric properties

Impedance spectroscopy was employed for studying the electrical properties of complex perovskite samples. From the measurements, it was readily apparent that all the compounds display characteristics typical of an insulating dielectric; high impedances and frequency-independent capacitances over the range 10^2–10^6 Hz (frequency dependences not shown). The dielectric constants κ were recorded at 100 kHz between 20 and 150 °C. They are plotted in Fig. 6 and summarized in Table 5. In agreement with previous reports [30,40], $Ba_3ZnTa_2O_9$ and $Ba_3MgTa_2O_9$ exhibited κ of ~22 and ~30, respectively, with small temperature dependences. The dielectric behaviors of the other five compounds have not so far been reported. Pb_2ScTaO_6 has the same octahedral composition as Ba_2ScTaO_6 but the presence of lone pair Pb^{2+} ion causes a clear ferroelectric behavior [41]. For $PbLaMgTaO_6$ [42] and $La_{5/3}MgTaO_6$ [35], the dielectric constants have been reported to be in the comparable ranges to those of $ALaMgTaO_6$ (A = Ba, Sr, Ca). All the seven compounds in Fig. 6 display somewhat similar temperature dependences of κ, but with significantly different magnitudes. The measured κ increases in the order M' = Mg < Zn < Sc, as clearly recognized from the comparisons between isostructural pairs Ba_2ScTaO_6 vs. $BaLaMgTaO_6$, and $Ba_3ZnTa_2O_9$ vs. $Ba_3MgTa_2O_9$. Such a composition dependence of κ presumably arises from the different polarizabilities of M' cations.

For the microwave dielectrics such as $Ba_3ZnTa_2O_9$ and $Ba_3MgTa_2O_9$, the loss $\tan\delta$ (or the quality factor $Q = 1/\tan\delta$) is a critical parameter for the technological utilizations. Usually their Q factors are assessed in the GHz range and are often presented as $Q \times f$ to compensate for the frequency dependence of Q. The continued research efforts in this field have now enabled the Q factors exceeding 10,000 ($\tan\delta = 0.0001$) to be routinely reproduced in various $Ba_3M^{2+}M_2^{5+}O_9$ type ceramics (Ref. [25] and references therein). In the present work the dielectric loss was evaluated as $\tan\delta = -Z'/Z''$, from the complex impedance $Z = Z' + iZ''$ measured at 100 kHz. Although our experimental conditions were not optimized in order to attain ideal ceramic sintering, the losses were observed to be fairly low in all the samples (Table 5). The measured $\tan\delta$ range 0.003–0.007 corresponds to the Q factors of 150–300, which could have been improved, perhaps dramatically, if the sample processing was optimized. For the complex perovskites, the point defects are regarded as an important source of the dielectric loss [40,43]. The pellet samples in this study are of 80–82% relative density and

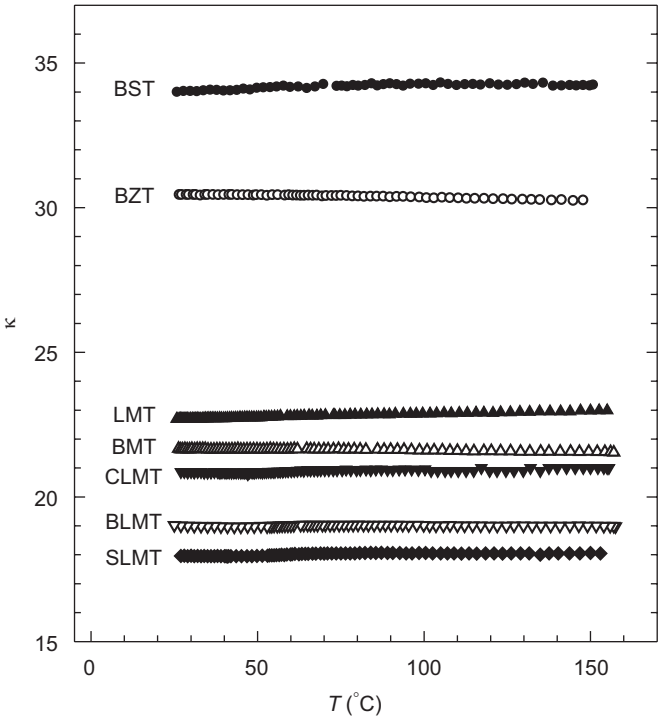

Fig. 6. Temperature-dependent dielectric constants of complex perovskite oxides containing Ta^{5+}. Compositions are abbreviated to same acronyms as in Fig. 1. Dielectric constant κ was evaluated from the measured capacitances using the sample dimensions at room temperature.

Table 5
Dielectric properties and electrical conductivity of complex perovskite oxides measured at room temperature and at 100 kHz

Compound	κ	$\tan\delta$	τ_C (ppm/K)[a]	σ_{el} (10^{-9} S/cm)
$BaLaMgTaO_6$	19.0	0.005	1±3	5.5
$SrLaMgTaO_6$	18.0	0.007	55±5	0.73
$CaLaMgTaO_6$	20.9	0.006	55±4	1.8
$La_2Mg(Mg_{1/3}Ta_{2/3})O_6$	22.7	0.004	98±1	0.62
$Ba_3MgTa_2O_9$	21.7	0.003	−37±2	0.24
$Ba_3ZnTa_2O_9$	30.4	0.004	−56±2	0.25
Ba_2ScTaO_6	34.0	0.004	54±6	9.0

[a] τ_C is evaluated for the temperature range 20–150 °C.

parts of the measured loss can be attributed to the imperfect sintering. Compared with other popular cations (Ti, Nb, or W) in the dielectrics, Ta has favorable aspects for the lower dielectric loss. Having a higher-lying valence *d* orbital, Ta shows little tendency towards the second-order Jahn–Teller distortion that can lead to ferroelectric behaviors [44]. In addition, Ta^{5+} ions are not prone to reduction under the usual oxide dielectric processing conditions. The cation reduction can create the charge carriers and anion defects that will serve as energy dissipation sites. This type of defect and the loss associated with it are more problematic in dielectrics based on Ti^{4+}, Nb^{5+}, or W^{6+}.

Small values for the temperature dependence of the resonance frequency (τ_f) and dielectric constants (τ_κ) are highly desirable in microwave dielectrics research [45]. They are related to each other through the expression $\tau_f = -[\alpha_L + (\tau_\kappa/2)]$, where α_L is the linear thermal expansion coefficient. τ_κ is also related to the temperature coefficient of capacitance, $\tau_C = C^{-1}(\partial C/\partial T)$, according as $\tau_\kappa = \tau_C - \alpha_L$ [46]. For most perovskite oxides, α_L is in the range of 5–12 ppm/K [47], and therefore the τ_κ of each compound in Table 5 might be estimated from the measured τ_C within the accuracy of ~10 ppm/K.

The origins of sign and magnitude of those temperature coefficients in different compounds are not completely understood. However, Reaney et al. [48] have proposed an empirical correlation between τ_κ and the perovskite tolerance factor and the onset of the octahedral tilting, using several Ba- and Sr-based complex perovskites. They showed that three distinct patterns of τ_κ variations exist according to the octahedral tilting modes. Compounds that are not distorted by octahedral tilting normally display negative values of τ_κ, whereas compounds with both in-phase and out-of-phase tilting distortions normally display positive values of τ_κ. Those which adopt intermediate tilt systems, where only out-of-phase tilting is observed, lie near the transition between the two regimes and often have small values of τ_κ.

Among the compounds studied here $Ba_3MgTa_2O_9$, and $Ba_3ZnTa_2O_9$ are not distorted by octahedral tilting and exhibit negative τ_C's as expected. The structures of $SrLaMgTaO_6$, $CaLaMgTaO_6$ and $La_2Mg(Mg_{1/3}Ta_{2/3})O_6$ show both out-of-phase and in-phase tilts (tilt system $a^-a^-c^+$, see Fig. 4) and exhibit positive values of τ_C in agreement with expectations. The positive τ_C value seen for Ba_2ScTaO_6 does not agree with expectations. The reasons for this are not clear, although presence of significant cation disorder may be a factor. The other cubic perovskite in Table 5, $BaLaMgTaO_6$, has a dielectric constant that is nearly temperature independent ($\tau_C = 1 \pm 3$ ppm/K) over the measured temperature interval. It is interesting to note that, in the τ_κ vs. *t* plot provided by Reaney et al. [48] the point of $\tau_\kappa = 0$ falls near the boundary between the non-tilt and the out-of-phase tilt regimes. While $BaLaMgTaO_6$ is cubic its tolerance factor ($t = 0.981$) suggests that an out-of-phase tilt distortion may be accessible upon lowering the temperature. The proximity of an octahedral tilting instability may be responsible for the exceedingly low value of τ_κ.

4. Conclusion

Crystal structures, optical band gaps, and dielectric properties of the complex perovskites $ALaMgTaO_6$ (A = Ba, Sr, Ca) and $La_2Mg(Mg_{1/3}Ta_{2/3})O_6$ are presented. As revealed by the synchrotron X-ray diffraction, the compounds show complete rock-salt type 1:1 ordering of the octahedral cations. The crystal symmetries are differentiated by tolerance factor, *t*. $BaLaMgTaO_6$ ($t = 0.981$), maintains a cubic symmetry while the other three compounds undergo $a^-a^-c^+$ octahedral tilting distortions that lead to monoclinic symmetry. Diffuse-reflectance spectroscopy reveals band gaps of 4.6–4.8 eV that are much larger than ternary tantalate perovskites like $KTaO_3$ ($E_g = 3.5$ eV). The increase in band gap results from electronic isolation of TaO_6 octahedra that leads to a reduction in the conduction bandwidth. The dielectric behaviors of $ALaMgTaO_6$ (A = Ba, Sr, Ca) and $La_2Mg(Mg_{1/3}Ta_{2/3})O_6$ at 20–150 °C are reported. The general characteristics of these compounds are low dielectric loss and reasonably low temperature coefficients. The dielectric properties of $BaLaMgTaO_6$ may be of particular interest because its dielectric constant ($\kappa = 19$) is nearly temperature independent ($\tau_C = 1 \pm 3$ ppm/K).

Acknowledgments

The authors acknowledge funding from the National Science Foundation through the Center for the Design of Materials (CHE-043567) and a Materials World Network Grant (DMR-0603128).

References

[1] M.T. Anderson, K.B. Greenwood, G.A. Taylor, K.R. Poeppelmeier, Prog. Solid State Chem. 22 (1993) 197.
[2] F.S. Galasso, Structure, Properties and Preparations of Perovskite-type Compounds, Pergamon Press, Oxford, 1969.
[3] R.H. Mitchell, Perovskites Modern and Ancient, Almaz Press, Thunder Bay, Ontario, 2002, pp. 88–91.
[4] P.K. Davies, Curr. Opin. Solid State Mater. Sci. 4 (1999) 467.
[5] S. Kawashima, M. Nishida, I. Ueda, H. Ouchi, J. Am. Ceram. Soc. 67 (1984) C59.
[6] S. Nomura, K. Toyama, K. Kaneta, Jpn. J. Appl. Phys. 21 (Part 2) (1982) L624.
[7] L.E. Cross, Ferroelectrics 76 (1987) 241.
[8] P.K. Davies, J. Tong, T. Negas, J. Am. Ceram. Soc. 80 (1997) 1727.
[9] I. Levin, J.Y. Chan, R.G. Geyer, J.E. Maslar, T.A. Vanderah, J. Solid State Chem. 156 (2001) 122.
[10] A.C. Larson, R.B. von Dreele, General structure analysis system (GSAS), Report LAUR 86-748, Los Alamos National Laboratory, NM, 1994.
[11] B.H. Toby, J. Appl. Crystallogr. 34 (2001) 210.
[12] I.P. Shapiro, Opt. Spektrosk. 4 (1958) 256.
[13] J.R. Macdonald, Impedance Spectroscopy, Wiley, New York, NY, 1987.

[14] M.W. Lufaso, P.W. Barnes, P.M. Woodward, Acta Crystallogr. B 62 (2006) 397.
[15] M.W. Lufaso, P.M. Woodward, Acta Crystallogr. B 57 (2001) 725.
[16] P.M. Woodward, Acta Crystallogr. B 53 (1997) 32.
[17] C.J. Howard, B.J. Kennedy, P.M. Woodward, Acta Crystallogr. B 59 (2003) 463.
[18] P.W. Barnes, M.W. Lufaso, P.M. Woodward, Acta Crystallogr. B 62 (2006) 384.
[19] M.T. Anderson, K.R. Poeppelmeier, Chem. Mater. 3 (1991) 476.
[20] M. Azuma, S. Kaimori, M. Takano, Chem. Mater. 10 (1998) 3124.
[21] T. Nakamura, J.-H. Choy, J. Solid State Chem. 20 (1977) 233.
[22] V.V. Fomichev, A.M. Frolov, V.B. Vyazovov, Zh. Neorg. Khim. 36 (1991) 3048.
[23] S. Kato, E. Ohmori, Y. Suzuki, Y. Ohshima, M. Sugai, H. Takizawa, T. Endo, J. Ceram. Soc. Jpn. 107 (1999) 209.
[24] J.-S. Kim, C.-I. Cheon, H.-J. Kang, H.-S. Shim, C.-H. Lee, S. Nam, J.-D. Byun, Mater. Lett. 38 (1999) 294.
[25] M.W. Lufaso, Chem. Mater. 16 (2004) 2148.
[26] S. Janaswamy, G.S. Murthy, E.D. Dias, V.R.K. Murthy, Mater. Lett. 55 (2002) 414.
[27] A.J. Jacobson, B.M. Collins, B.E.F. Fender, Acta Crystallogr. B 32 (1976) 1083.
[28] B.E. Warren, X-ray Diffraction, Dover Publications, New York, NY, 1990, pp. 206–216.
[29] R.D. Shannon, Acta Crystallogr. A 32 (1976) 751.
[30] S.B. Desu, H.M. O'Bryan, J. Am. Ceram. Soc. 68 (1985) 546.
[31] T. Sekiya, T. Yamamoto, Y. Torii, Bull. Chem. Soc. Jpn. 57 (1984) 1859.
[32] J.-H. Park, P.M. Woodward, J.B. Parise, Chem. Mater. 10 (1998) 3092.
[33] L. Dupont, L. Chai, P.K. Davies, Mater. Res. Soc. Symp. Proc. 547 (1999) 93.
[34] M.C. Knapp, P.M. Woodward, J. Solid State Chem. 179 (2006) 1076.
[35] D.D. Khalyavin, A.M.R. Senos, P.Q. Mantas, D.N. Argyriou, I. Tarroso Gomes, L.G. Vieira, J.L. Ribeiro, J. Solid State Chem. 180 (2007) 41.
[36] I.D. Brown, R.D. Shannon, Acta Crystallogr. A 29 (1973) 266.
[37] J.-H. Park, P.M. Woodward, Int. J. Inorg. Mater. 2 (2000) 153.
[38] H.W. Eng, P.W. Barnes, B.M. Auer, P.M. Woodward, J. Solid State Chem. 96 (2003) 535.
[39] W.A. Harrison, Electronic Structure and the Properties of Solids, W.H. Freeman and Company, San Francisco, CA, 1980.
[40] T. Kolodiazhnyi, A. Petric, A. Belous, O. V'yunov, O. Yanchevskij, J. Mater. Res. 17 (2002) 3182.
[41] N. Setter, L.E. Cross, J. Appl. Phys. 51 (1980) 4356.
[42] J.K. Montgomery, M.A. Akbas, P.K. Davies, J. Am. Ceram. Soc. 82 (1999) 3481.
[43] G. Rong, N. Newman, B. Shaw, D. Cronin, J. Mater. Res. 14 (1999) 4011.
[44] K.M. Ok, P.S. Halasyamani, D. Casanova, M. Llunell, P. Alemany, S. Alvarez, Chem. Mater. 18 (2006) 3176.
[45] I.M. Reaney, P. Wise, R. Ubic, J. Breeze, N.McN. Alford, D. Iddles, D. Cannell, T. Price, Philos. Mag. A 81 (2001) 501.
[46] E.L. Colla, I.M. Reaney, N. Setter, J. Appl. Phys. 74 (1993) 3414.
[47] D. Taylor, Br. Ceram. Trans. J. 84 (1985) 181.
[48] I.M. Reaney, E.L. Colla, N. Setter, Jpn. J. Appl. Phys. 33 (1994) 3984.